HHS Public Access

Author manuscript

J Bone Miner Res. Author manuscript; available in PMC 2024 November 01.

Published in final edited form as:

J Bone Miner Res. 2023 November ; 38(11): 1560–1576. doi:10.1002/jbmr.4902.

Cannabidiol and cannabigerol, non-psychotropic cannabinoids, as analgesics that effectively manage bone fracture pain and promote healing in mice

Deepak Kumar Khajuria[a,b], **Vengadeshprabhu Karuppagounder**[a,b], **Irena Nowak**[a,b], **Diana E. Sepulveda**[c,d], **Gregory S. Lewis**[a,b], **Christopher C Norbury**[e], **Wesley M. Raup-Konsavage**[c], **Kent E. Vrana**[c], **Fadia Kamal**[a,b,c,*], **Reyad A. Elbarbary**[a,b,f,g,*]

[a]Department of Orthopaedics and Rehabilitation, The Pennsylvania State University College of Medicine, Hershey, Pennsylvania 17033, USA

[b]Center for Orthopaedic Research and Translational Science (CORTS), The Pennsylvania State University College of Medicine, Hershey, Pennsylvania 17033, USA

[c]Department of Pharmacology, The Pennsylvania State University College of Medicine, Hershey, Pennsylvania 17033, USA

[d]Department of Anesthesiology and Perioperative Medicine, The Pennsylvania State College of Medicine, Hershey, Pennsylvania 17033, USA

[e]Department of Microbiology and Immunology, The Pennsylvania State University College of Medicine, Hershey, Pennsylvania 17033, USA

[f]Department of Biochemistry and Molecular Biology, The Pennsylvania State University College of Medicine, Hershey, Pennsylvania 17033, USA

[g]Center for RNA Molecular Biology, Pennsylvania State University, University Park, Pennsylvania 16802, USA

Abstract

Bone fractures are among the most prevalent musculoskeletal injuries, and pain management is an essential part of fracture treatment. Fractures heal through an early inflammatory phase, followed by repair and remodelling. Nonsteroidal anti-inflammatory drugs (NSAIDs) are not recommended for fracture pain control as they potently inhibit the inflammatory phase and, thus, impair the healing. Opioids do not provide a better alternative for several reasons, including abuse potential. Accordingly, there is an unmet clinical need for analgesics that effectively ameliorate post-fracture pain without impeding the healing. Here, we investigated the analgesic efficacy of two non-psychotropic cannabinoids, cannabidiol (CBD) and cannabigerol (CBG), in a mouse model for tibial fracture. Mice with fractured tibiae exhibited increased sensitivity to mechanical, cold, and hot stimuli. Both CBD and CBG normalized pain sensitivity to all tested stimuli, and their analgesic effects were comparable to those of the NSAIDs. Interestingly, CBD and CBG

[*]Corresponding authors Reyad A. Elbarbary (relbarbary@pennstatehealth.psu.edu); Fadia Kamal (fkamal@pennstatehealth.psu.edu).

Conflict of interests

The authors declare no conflict of interest.

promoted bone healing via multiple mechanisms during the early and late phases. During the early inflammatory phase, both cannabinoids increased the abundance of periosteal bone progenitors in the healing hematoma and promoted the osteogenic commitment of these progenitors. During the later phases of healing, CBD and CBG accelerated the fibrocartilaginous callus mineralization and enhanced the viability and proliferation of bone and bone-marrow cells. These effects culminated in higher bone volume fraction, higher bone mineral density, and improved mechanical quality of the newly formed bone. Together, our data suggest CBD and CBG as therapeutic agents that can replace NSAIDs in managing post-fracture pain as both cannabinoids exert potent analgesic effects and, at the same time, promote bone healing.

Keywords

Fracture healing; bone regeneration; analgesic; cannabidiol; cannabigerol

Introduction

Bone healing proceeds through a sequence of overlapping processes that can be divided into three main phases: inflammation, repair, and remodeling [1,2]. The inflammatory phase initiates bone repair via the formation of a hematoma that is rich in immune cells. The microenvironment in the healing hematoma induces immune cells to secret high levels of cytokines, growth factors, and angiogenic factors [1,2]. These factors are vital for neovascularization as well as recruitment of mesenchymal stem cells (MSCs) and bone progenitors that are required for bone regeneration [1,2]. The repair of most of cortical bone fractures proceeds via the initial formation of a fibrocartilaginous (soft) callus that is filled with proliferating chondrocytes [1,2]. These chondrocytes undergo hypertrophy and mineralization at later stages of the repair phase, which hardens the cartilaginous area that bridges the fracture gap and allows new blood vessels to invade the mineralized soft callus [1,2]. The mineralized soft callus is then replaced by newly formed woven bone to form the bony callus, which undergoes remodeling to re-establish the characteristic laminar structure of the cortical bone [1,2].

Bone fracture results in distortion and damage of the mechanosensitive nerve fibers that innervate the bone, leading to development of the initial sharp pain sensation experienced by fracture patients [16]. The stromal and immune cells that populate the fracture site to initiate the repair process secret neurotransmitters, growth factors, and cytokines. These factors cause ectopic nerve sprouting, which exacerbates pain sensation, resulting in restricted patient movement. As effective healing of a load-bearing bone (such as the femur or the tibia) requires proper movement-induced loading of the injured bone within the tolerable limits, inappropriate pain management results in suboptimal bone loading and, hence, delayed healing [16]. NSAIDs and opioids are currently used to manage fracture pain [17,18]. Pre-clinical and clinical studies indicate that NSAIDs, including indomethacin and celecoxib, inhibit bone repair mainly via inhibiting the inflammatory phase of the repair process [4–10]. There are several factors that remain unclear with regard to the use of NSAIDs in fracture patients, including the dose and treatment duration of the NSAID that can be safely used. Generally, many orthopedic surgeons believe that NSAIDs are

contraindicated in bone fracture patients [4,17,19–22]. Opioids do not offer a better alternative as they interfere with the functional status of the patients and their ability to go back to work [11]. Importantly, recent studies have also shown that opioids increase the risk of bone fracture and delay bone healing [14,23]. These drawbacks of the available analgesics are among the reasons that bone fracture patients fail to participate in an effective rehabilitation program [4,17,19–22]. Accordingly, managing pain in fracture patients remains an unmet clinical problem that awaits the discovery of potent analgesics with minimal negative impact on the healing process [15]. In this regard, there is an increasing interest in the potential therapeutic uses of phytocannabinoids, and alleviating pain is one area where cannabinoids hold great therapeutic promise [24]. However, the potential of cannabinoids in managing fracture pain has not been investigated so far, and, generally, the lack of scientific evidence for the efficacy of cannabinoids in different applications hinders their clinical prescription.

Cannabidiol (CBD) is a non-psychotropic cannabinoid and one of the major constituents of cannabis [24]. In 2018, pure CBD was approved by the FDA for treatment of seizures in pediatric patients with Lennox-Gastaut or Dravet syndrome [24]. Thus, the safety profile and the pharmacokinetics of pure CBD when used in human patients are well characterized, which facilitates CBD repurposing to other medical indications. Only a few studies investigated the impact of CBD on fracture healing and bone homeostasis. One study reported that CBD enhances the biomechanical properties of the newly formed bone in a rat fracture model [25], and another study demonstrated that CBD attenuates bone loss in a rat model of spinal cord injury-induced bone loss [26]. Hence, there is dearth of information with regard to whether CBD affects bone healing in species other than rat as well as the pathways whereby CBD impacts bone homeostasis and regeneration. CBG is another non-psychotropic cannabinoid that is gaining growing attention recently [27]; yet, its impact on bone health and repair has never been investigated.

Here, we use a mouse model of endochondral fracture healing to assess the analgesic efficacy of CBD and CBG in post-fracture pain and compare their analgesic effects to those of NSAIDs. Importantly, we investigate the impact of CBD and CBG on the different phases of healing and assess their impact on the proliferation, viability and homeostasis of bone progenitors, bone cells, and soft-callus chondrocytes. In parallel, we assess the influence of CBD and CBG on the structure and quality of the newly formed bone.

Materials and Methods

Animals

Adult male C57BL/6J mice (stock # 000664) at 14 weeks of age were purchased from the Jackson Laboratory (Bar Harbor, ME, USA) and allowed to acclimate for 2 weeks. The mice were then subjected to tibial fracture surgeries (at the age of 4 months; average weight was ~30 gm). The B6N.Cg-Tg(Pdgfra$^{cre/ERT}$) 467Dbe/J (stock # 018280) and B6.Cg-*Gt(ROSA)26Sor*$^{tm9(CAG-tdTomato)Hze}$/J (known as Ai9) (stock # 007909) mice were purchased from the Jackson Laboratory. Ai9 is a Cre reporter strain that have a *loxP*-flanked STOP cassette, which prevents the transcription of a red fluorescent protein variant (tdTomato). Pdgfra^{Ai9} mice were obtained by breeding male Pdgfra^{Ai9} mice with female Ai9 mice and backcrossing for five times. When Pdgfra^{Ai9} mice were injected

with tamoxifen, the Cre was activated and removed the STOP cassette; subsequently, the PDGFRα^{+} cells were labeled with tdTomato. All mice were provided with ad libitum access to chow and water, and they were housed in ventilated cages with bedding at a temperature of 21.1°C to 22.8°C, and 30% to 70% humidity (12-hour light/dark cycle). All animal protocols were approved by the University Committee on Animal Resources (IACUC) at the Pennsylvania State University College of Medicine.

Mid-diaphysis tibial fracture surgery, drug injection, and tissue harvest

Mice were anesthetized by administering a mixture of ketamine (100 mg/kg) and xylazine (10 mg/kg) (i.p.), and open mid-diaphyseal tibial fractures were induced in the right hindlimb as previously described [2,28,29]. An intramedullary nail was used to stabilize the fracture. X-ray images were collected postoperatively and at the harvest time to confirm proper alignment of the fracture site. The mice received an i.p. injection of 5 mg/kg/day of CBD (Cayman) or CBG (Cayman), 2.5 mg/kg/day of indomethacin (Sigma Aldrich), or 3 mg/kg/day of celecoxib (Sigma Aldrich). All treatments commenced 24 h post-fracture and continued until the harvest time. The dose of CBD, CBG, indomethacin, or celecoxib was determined based on previous publications [25,30–33]. All the drugs were dissolved in a vehicle composed of DMSO, Tween 80, and saline (1:1:18), and the control mice received a daily injection of the same vehicle. The PDGFRα^{Ai9} mice received a daily i.p. injection of 100mg/kg tamoxifen (Sigma Aldrich) for 5 successive days; on the sixth day, the mice underwent the fracture surgeries [34].

At the harvest time, the animal was euthanized, and the fractured hindlimb was harvested from the mid-femur to the tibiotalar joint to avoid disturbing the callus tissue. Most of the surrounding soft tissues were removed with care not to disturb the fracture site. For day 28 samples, the intramedullary pin was removed, and the bone was wrapped in phosphate buffered saline (PBS)-soaked gauze and frozen at −20° C. Samples were subjected to micro-computed tomography (μC) analysis followed by biomechanical testing. For d14 and d21 samples, the isolated bone was fixed in 10% (v/v) neutral buffered formalin (Thermo Fisher Scientific), the intramedullary pin was then removed, and samples were subjected to μCT analysis. Following μCT, samples were decalcified in 14% w/v EDTA tetrasodium (Thermo Fisher Scientific), processed, and embedded in paraffin for immunofluorescence (IF) and histological staining. The harvest timepoints were determined based on studies that have been published by us and others about the time course of healing in this model [2,28,29].

Mass Spectrometry

Serum was isolated from the treated mice, and the plasma concentrations of CBD and CBG were determined using a Sciex QTRAP 6500+ mass spectrometer coupled with a Sciex EXion HPLC separation system as we detailed previously [35,36].

Pain test

The von Frey, acetone drop, and hot plate (52 °C) tests were performed as we and others described previously [36,37]. For the von Frey test, the threshold required to elicit a withdrawal response was recorded; while for the acetone drop and hot plate tests, the time required to elicit a nociceptive behavior (paw withdrawal or paw licking) was recorded. All

tests were performed 1 hr following administration of the drug or the vehicle. The tests were performed in the following order to prevent iatrogenic effects: von Frey (d4), acetone drop test (d5), and hot plate (d6). All tests were performed by researchers who were blind to the treatment.

Gait analysis

The gait analysis was performed as we described previously [36]. Briefly, the mice were placed at one end of a 3-foot-long, dark tunnel that was lined with a blank paper, and the rear legs of the mice were stamped on an ink pad. The mice left a trace of footprints as they crossed to the other end of the tunnel. Using these footprints, four separate gait metrics (stride, stance, sway, and intensity of paw print) were recorded and quantified by researchers who were blind to the treatment. For each mouse, the experiment was repeated 3 times, and at least 10 measurements were taken for each experiment. The intensity of the paw print was quantified using ImageJ.

Histological staining, histomorphometry, and TUNEL assay

Sagittal sections with thicknesses of 5 μm that spanned the center of the callus were collected and stained with Hematoxylin/Safranin-O/Fast Green or Masson's trichrome as previously described [2,28]. Osteoblasts (cuboidal mononuclear cells located on bone surfaces) were counted, and the number was normalized to bone surface area using the OsteoMeasure system (OsteoMetrics Inc.) as described previously [38–40]. TUNEL assay was performed using an Invitrogen™ Click-iT™ Plus TUNEL Assay Kit for In Situ Apoptosis Detection (Catalog # C10619, Fisher Scientific) according to the manufacturer's instructions, and imaging and analysis were performed as described under IF staining (below).

IF staining

IF staining was performed as we previously detailed [2,29,41–43] (all antibodies are listed in Table S1). Mounting and nuclear staining were performed using ProLongTM Gold antifade reagent with DAPI (Invitrogen). Images were captured using Zeiss Axio Observer 7 upright wide-field microscope (Carl Zeiss Microscopy GmbH), and image analysis was performed using Zen Blue advanced image analysis software. For extracellular matrix proteins, the stained area of the analyzed protein was normalized to the total area of the region of interest (either the soft callus or the woven bone). For intracellular proteins, the number of cells that expressed the analyzed protein was normalized to the total number of cells in the region of interest (defined as $DAPI^+$ cells).

μCT analysis

μCT analysis was performed as we detailed previously [44]. Briefly, samples were scanned using a vivaCT 40 (Scanco) at 55 kVp, 145 mA, 300 ms integration time, and 10.5-micron isometric voxels. A hydroxyapatite-based phantom (QRM, Möhrendorf Germany) was included in each scan. Image stacks were imported into Scanco (Evaluation Program v6.6) for analysis. Images were filtered with a Gaussian filter, then each sample was cropped. The center plane of the fracture callus was determined using the transverse image slices,

and the volume of interest (VOI) was defined based on the proximal and distal ends of the callus, which were discernable at the analyzed timepoints. Images were contoured to outline the callus, excluding the native bone cortex. The analyzed VOI averaged approximately 550 slices for d14 and 450 slices for d21 and d28. The total callus segmentation was inspected through all slices. Mineralized portions of the callus were further segmented based on a threshold of 250 mgHA/ccm. Bone volume fraction (BV/TV), mean bone mineral density (BMD), trabecular thickness (Tb.Th), trabecular number (Tb.N), trabecular separation (Tb.Sp), and connectivity density (Conn.D) were determined. 3D reconstruction was performed by importing DICOM (Digital Imaging and Communications in Medicine) stacks into Avizo 3D software (Thermo Fisher Scientific, Waltham MA). Scanning and analysis were performed in a manner blinded to the treatment.

Biomechanical testing

Blinded biomechanical testing was performed as previously described [2,28] with few modifications. Briefly, each sample was potted on each end with polymethylmethacrylate dental cement (Ortho-Jet BCA, Lang Dental, Wheeling IL) into a 6 mm x 6 mm square aluminum tubing. A custom fixture was used to align the pots with the bone's long axis, with a 7 mm gauge length between the pots. The potted specimen was rehydrated in PBS and fastened to an MTS/Interlaken servohydraulic axial-torsion load frame with a 177 Nmm load cell. Torsion was applied at a rate of 1°/s until failure, and the maximum torque was recorded. Stiffness was also determined as the slope of the initial linear portion of the torque vs. rotation plot.

Flow cytometry

The mice were sacrificed on d3, and the healing hematoma was collected from each mouse (avoiding the surrounding cortical bone); four calli were pooled for each FC run. The contralateral, unfractured tibia was also collected from each mouse, the BM was completely flushed out, and each of the bone and the BM was processed and analyzed separately. The soft tissues were completely removed from the collected calli and bones, the tissues were minced, and then digested for 1 h at 37° C in a mixture of collagenase/dispase (1 μg/ml, catalog: 10269638001, Roche) and collagenase D (3 mg/ml, catalog: 11088882001, Roche). The red blood cells were lysed using 1X RBC lysis buffer (Catalog # 00–4333-57, eBioscience) according to the manufacturer's protocol. The cells were then counted, blocked using 24G2 hybridoma and 20% serum, and stained using the antibodies described in Table S2. Isotype controls and fluorescence-minus-one (FMO) controls were employed. The cells were sorted using 23-color BD FACS Symphony (BD Biosciences, San Jose, CA), and the results were analyzed using FlowJo Software 10.6.2 (Treestar, Ashland, OR).

In-vitro differentiation of periosteal progenitors

The $CD45^{-}CD31^{-}PDGFR\alpha^{+}$ cells were isolated using fluorescence-activated cell sorting (FACS) and the same protocol and equipment described above for FC (the primary antibodies are given in Table S2). The isolated primary cells were then cultured in StemXVivo Osteogenic/Adipogenic Base Media (R & D). At 50–70% confluency, osteogenic differentiation was induced by the addition of StemXVivo Mouse/Rat Osteogenic Supplement (R & D). The differentiation medium was changed every 3 days for 2 weeks.

Statistical analyses

The sample size was calculated by 'pwr2' R package; power and significance levels were provided as 0.8 and 0.05, respectively. The calculated sample size was 7 for biomechanical testing (expected effect 30%), and 5 for the rest of experiments (expected effect 44%). The experimental groups were populated accordingly. The unpaired Student's *t* test was used to determine statistical significance between two groups, whereas ANOVA (followed by Tukey's post hoc test) was used to determine statistical significance among three or more groups. Statistical analyses were performed using the GraphPad Prism software. The following symbols were used to indicate significance: (*) $P < 0.05$; (**) $P < 0.01$; (***) $P < 0.001$; (****) $P < 0.0001$.

Results

The plasma concentrations of CBD and CBG are comparable following either acute or chronic administration

To study the therapeutic effects of CBD and CBG on fracture healing, we induced open, mid-diaphyseal tibial fracture in 4-month-old mice according to the standard protocol [2,28] (Fig. 1A). The mice then received 5mg/kg/day (i.p.) of CBD or CBG; injections commenced 24 h post-fracture and continued until the harvest time (Fig. 1B). Thirty minutes following the administration of the first dose, the plasma concentration of CBD or CBG was ~40 ng/ml, and the concentration decreased to ~10 ng/ml in two hours (Fig. 1C, D). The steady-state concentration of either CDB or CBG following daily administration for three or four weeks was ~100–150 ng/ml (Fig. 1E).

CBD and CBG alleviate hypersensitivity to mechanical, cold, and hot stimuli in mice with tibial fracture

To determine the impact of CBD or CBG on fracture-associated pain, we performed a set of pain behavior tests. We first tested changes in the mechanical nociception in response to CBD or CBG treatment by performing the von Frey test, during which we pressed a microfilament against the paw of the fractured leg and measured the threshold that was needed to evoke a withdrawal response [36]. The vehicle-treated fractured mice exhibited mechanical allodynia as indicated by ~3-fold reduction in the response threshold relative to its level in the sham-operated mice (Fig. 2A). Treatment with CBD or CBG alleviated the observed mechanical allodynia and increased the response threshold in the fractured mice to a level comparable to that measured in the sham-operated mice (Fig. 2A). Importantly, the effects of CBD and CBG on mechanical allodynia were comparable to those of indomethacin and celecoxib, which are widely used NSAIDs that we employed as positive controls (Fig. 2A).

We also tested for increased sensitivity to cold and hot stimuli by performing the acetone evaporation test and the hot plate test, respectively. Compared to the sham groups, the vehicle-treated fractured mice exhibited hypersensitivity to both stimuli as evidenced by ~3-fold reduction in the time required to elicit a nociceptive response (Fig. 2B, C). Treatment with CBD, CBG, indomethacin, or celecoxib ameliorated this hypersensitivity and increased

response times in both tests to their values in the sham groups (Fig. 2B, C). These results indicate that CBD and CBG ameliorate post-fracture pain as effectively as NSAIDs.

As expected, the tibial fracture impaired the gait of mice, resulting in shortened stride length (Fig. 2D), stance length (Fig. 2E), and sway distance (Fig. 2F), and reduced the paw print intensity (Fig. 2G). Treatment with CBD, CBG, indomethacin, or celecoxib significantly recovered all gait parameters (Fig. 2D-GF). The only exception was the failure of celecoxib to enhance the sway distance (Fig. 2F).

CBD and CBG accelerate the mineralization of the soft callus

To assess the impact of CBD or CBG on the repair phase of fracture healing, we first analyzed day 14 post-fracture (d14). As we and others reported previously [2,28], the callus of d14 in the vehicle-treated group was composed of a fibrocartilaginous callus surrounded by woven bone (Fig. 3A; Fig. S1A, B). The fibrocartilaginous callus occupied the area within and in close vicinity of the fracture line, while the woven bone filled the callus areas distal to the fracture line (Fig. 3A; Fig. S1A, B). As expected at this stage of healing, the chondrocytes of the fibrocartilaginous expressed high levels of the chondrocyte pre-hypertrophy marker Indian hedgehog (IHH) (Fig. 3B) and the hypertrophy markers Collagen 10 (Col X) (Fig. 3C) and matrix metallopeptidase 13 (MMP13) (Fig. S1C). In addition, in the regions where the fibrocartilaginous callus fused with the surrounding woven bone, a subset of hypertrophic chondrocytes expressed Collagen I (Col I) (Fig. 3A) and osteocalcin (OC) (Fig. 3D), which are both essential proteins for the mineralization of the soft callus [1,2]. Furthermore, ~30% of the chondrocytes expressed SP7 (also known as osterix) (Fig. 3E), a transcription factor that induces the expression of Col I and bone gamma carboxyglutamate protein (Bglap, the gene that encodes OC) [45,46]. Also, SP7 expression in the chondrocytes plays important roles in the endochondral bone formation [47]. Treatment with either CBD or CBG did not result in any significant differences in the expression of IHH (Fig. 3B), Col X (Fig. 3C) or MMP13 (Fig. S1C), which indicates normal chondrocyte hypertrophy. However, the fibrocartilaginous callus in the mice that were treated with CBD or CBG exhibited ~2–3-fold increases in the expression of Col I (Fig. 3A), OC (Fig. 3D), and SP7 (Fig. 3E). Taken together, these data suggest that treatment with either CBD or CBG induces the expression of the factors that mediate soft-callus mineralization and endochondral ossification.

CBD and CBG augment woven bone formation

We next analyzed the woven bone area in the callus of d14 using μCT. We found that the calli of the CBD- or CBG-treated mice exhibited more BV/TV, BMD, Tb.Th, and Tb.N than the calli of the vehicle-treated mice (Fig. 4A, B). These results indicate that CBD and CBG promoted bone formation. Consistently, treatment with CBD or CBG enhanced the expression of Col I in the woven bone region (Fig. 5A), increased the number of osteoblasts per woven-bone surface area (Fig. 5B), and reduced the level of apoptosis in the region of woven bone (i.e., bone cells and bone marrow (BM) cells) (Fig. 5C).

CBD and CBG accelerate bony bridging of the fracture gap

We next analyzed the calli isolated from the different treatment groups on d21 post-fracture. At this time point, the fracture callus of the vehicle-treated mice was filled by newly formed woven bone, and the soft callus was nearly completely resorbed (Fig. S3A). μCT analysis indicated that the BV/TV, BMD, Tb.Th and Tb.N remained higher in the calli of the mice that were treated with CBD or CBG compared to the calli of the vehicle-treated mice (Fig. 6A, B). Consistent with the results on d14, treatment with CBD or CBG increased the number of osteoblasts per bone surface area (Fig. 6C). Furthermore, treatment with CBD or CBG induced the proliferation of osteoblasts/bone lining cells and BM cells (Fig. 6D). The number of apoptotic cells was comparable in all groups (Fig. S2B). Notably, the woven bone area of the vehicle-treated mice contained fewer apoptotic cells on d21 than on d14 (Fig. 5C; Fig. S2B).

CBD and CBG enhance the biomechanical properties of the healed bone

To analyze the impact of CBD or CBG on bone repair at the late stages of healing, we performed μCT analysis and biomechanical testing on calli collected on d28 post-fracture. The calli of CBD- or CBG-treated mice exhibited higher BV/TV, BMD, and Tb.Th, and lower Tb.Sp than the calli of the vehicle-treated mice (Fig. 7A, B). Also, biomechanical testing demonstrated that treatment with CBD or CBG substantially increased the biomechanical strength of the healed bone (Fig. 7C). No significant difference in the stiffness was observed among the 3 groups (Fig. 7C). Taken together with the results from days 14 and 21, these data indicate that CBD and CBG promote bone formation and fracture repair throughout the healing process.

PDGFRα^{+} periosteal progenitors express both CNR1 and CNR2

As our results indicate that CBD and CBG enhance bone formation (Figs 3–7), we next investigated whether they impact bone progenitors. Growing evidence indicates the involvement of periosteal precursors in fracture healing. Recently, periosteal PDGFRα^{+} progenitors have been identified as a major player in fracture healing [34]. Accordingly, we bred PDGFRα^{Cre} mice with Ai9 mice to produce the PDGFRα^{Cre}:Ai9 (hereafter will be referred to as PDGFR^{Ai9}) mice. We injected these mice with tamoxifen to label PDGFRα^{+} cells with tdTomato (see Materials and Methods) and detected high reporter activity in the periosteum of intact, unfractured bone (Fig. 8A), which is consistent with the published studies [34]. We further confirmed these observations using flow cytometry (FC) and found that the proportion of the PDGFRα^{+} cells in the nonhematopoietic and nonendothelial (CD45^{-} CD31^{-}) population was ~15-fold higher in the intact bone (devoid of BM) than in the BM (Fig. 8B). When we induced open mid-diaphyseal tibial fracture in the PDGFRα^{Ai9} mice and traced the tdTomato reporter activity in the healing callus 21 days post-fracture (Fig. S3), we detected tdTomato in the majority of the newly formed bone cells (Fig. 8C). These data demonstrate that the periosteal PDGFRα^{+} cells are a reservoir for progenitors that play central roles in bone formation during fracture healing, which is in total agreement with the published reports [34]. Based on these data, we focused our subsequent analyses on the PDGFRα^{+} progenitors (i.e., CD45^{-}CD31^{-}PDGFRα^{+} cells).

The cannabinoid receptor 1 (CNR1) and CNR2 are the major and most studied cannabinoid receptors. Using FC, we analyzed the expression of CNR1 and CNR2 on PDGFRα$^+$ progenitors that were isolated from the callus of d3, the contralateral intact bone, or the BM. The results indicated that the PDGFRα$^+$ progenitors are a heterogenous population that can be stratified into different subpopulations based on the expression of CNR1 and CNR2 (Fig. 8D). The subset of the progenitors that expressed CNR1, but not CNR2, was undetectable in the BM, but constituted a small % (~5%) of the progenitors in the intact bone and the callus (Fig. 8D). Importantly, while < 5% of the progenitors that were isolated from the BM co-expressed CNR1 and CNR2, ~20–30% of the progenitors that were isolated from the unfractured bone and the callus showed the co-expression of CNR1 and CNR2 (Fig. 8D). These data demonstrate specific enrichment of the PDGFRα$^+$ progenitors that express CNR1 in bone and fracture callus. The high similarity observed between the periosteal and callus, but not BM, progenitors with regard to the expression pattern of CNR1 and CNR2 provides further evidence that the periosteum is a major source of the callus-infiltrating progenitors.

Treatment with either CBD or CBG increases the abundance of the PDGFRα$^+$ progenitors during the early phases of healing

We isolated the d3 calli from mice that were treated with either the vehicle, CBD, or CBG, and we quantified the proportion of the PDGFRα$^+$ progenitors in the calli of each group using FC. The results indicated that treatment with CBD or CBG increased the abundance of the PDGFRα$^+$ progenitors ~3–4 fold (Fig. 9A). Furthermore, when we differentiated the PDGFRα$^+$ progenitors *in vitro* in the presence of vehicle, CBD, or CBG, both CBD and CBG promoted the osteogenic commitment of the progenitors and enhanced the formation of mineralizing bone cells (Fig. 9B). Taken together, CBD and CBG increased the number of bone progenitors during the early phases of healing and promoted the osteogenic differentiation of these progenitors. These data unravel a mechanism whereby CBD and CBG promote bone formation during fracture healing.

Discussion

We propose the FDA-approved cannabinoid CBD and the investigational cannabinoid CBG as therapeutic agents that not only attenuate post-fracture pain efficiently, but also promote bone healing. Our results demonstrate that mice with fractured tibiae exhibited impaired gait (Fig. 2D-G) and hypersensitivity to mechanical, cold, and hot stimuli (Fig. 2A-C). Treatment with the NSAID indomethacin or celecoxib normalized the gait and alleviated pain sensitivity in the fractured mice (Fig. 2A-G). CBD and its derivative dihydroxy-CBD have been reported to suppress chronic neuropathic and persistent inflammatory pain [(48)]. Derivatives of CBG have been also reported to possess anti-inflammatory and analgesic properties [(32)]. However, the analgesic potential of CBD or CBG in the context of post-fracture pain has never been investigated. The results we are reporting here demonstrate that CBD and CBG are as effective as the NSAIDs in normalizing pain sensitivity in the fractured limb (Fig. 2A-G). It is noteworthy that mice with fractured tibiae that were treated with either CBD or CBG displayed normalized gait parameters, reflecting better loading

of the fractured hindlimb relative to the vehicle-treated mice (Fig. 2G). This might have contributed to the improved healing observed in the cannabinoid-treated groups (Figs 3–7).

Both the innate and the adaptive immune systems play crucial roles in bone healing [3]. Modulation of the immune response by CBD is well studied. A considerable body of *in-vitro* and *in-vivo* studies indicate anti-inflammatory and immunosuppressive effects of CBD that involve both the innate and the adaptive responses [49]. On the contrary, several other studies have shown immunostimulatory and pro-inflammatory effects of CBD [49]. In general, the impact of CBD on the immune response/inflammation depends on several factors, which include the tissue/system in which CBD is studied, whether CBD is studied in healthy or disease conditions [50], and, importantly, the administered dose/concentration of CBD. Although the immunomodulatory effects of CBG are far less studied than those of CBD, CBG derivatives have also been shown to modulate inflammation and immune response [32,51]. Our study did not directly address the impact of CBD or CBG on the inflammatory/immune response during the healing process; however, our data clearly demonstrate that neither CBD nor CBG modulated the inflammatory response in a way that negatively impacted the healing (Figs 3–7). In fact, as early as d3 post-fracture, the modulatory effects of either CBD or CBG on the microenvironment of the fracture hematoma favored the proliferation and/or recruitment of the periosteal PDGFRα$^+$ progenitors (Fig. 9A). This positive impact of CBD or CBG on the healing process was sustained throughout the later phases of healing (Fig. 3–7).

CNR1 and CNR2 are the major and most studied cannabinoid receptors. Both CNR1 and CNR2 are expressed on chondrocytes, osteoblasts, osteocytes, and osteoclasts, although the expression level of CNR1 on bone cells is reported to be low [52–56]. Our data indicate that the PDGFRα$^+$ periosteal progenitors express both CNR1 and CNR2 (Fig. 8D). PDGFRα$^+$ progenitors constitute a small % of total bone cells (Fig. 8B), which is not surprising given that osteocytes alone constitute ≥ 90% of bone cells; however, PDGFRα$^+$ progenitors play crucial roles in bone repair [34] (Fig. 8C). Our single-cell analysis indicated that the expression of CNR1 and CNR2 is not uniform among PDGFRα$^+$ progenitors (Fig. 8D), which highlights the importance of single-cell analysis in investigating CNR1 and CNR2 expression in any given cell population. This heterogeneity in CNR1 and CNR2 expression among PDGFRα$^+$ progenitors would have been completely masked if the total RNA or total protein was analyzed. Interestingly, the number of progenitors that co-express CNR1 and CNR2 was significantly higher in the periosteum or the fracture callus than in the BM (Fig. 8D). This might be due to either stimulated expression of the receptors or increased proliferation of PDGFRα$^+$ progenitors that express both receptors in response to local bone/callus signals. The mechanism whereby CNR1 signaling regulates bone biology remains controversial. According to published studies, the impact of CNR1 signaling on bone homeostasis might be partially indirect through the inhibition of noradrenaline release from nerve terminals that are located close to the osteoblasts, which alleviates the noradrenaline-mediated inhibition of osteoblast activity [54]. The elevated expression of CNR1 that we identified in the periosteal and callus progenitors suggests a possible regulatory role for CNR1 in bone formation and remodeling by affecting the osteogenic potential of bone progenitors. This is an interesting point for future studies.

Generally, CBD exhibits low affinity to CNR1 and CNR2 [57,58]; further, some of the physiological effects of CBD have been reported to be independent of CNR1 and/or CNR2 [59–61]. However, CBD can also signal through CNR1 and/or CNR2 via indirect mechanisms that involve inhibiting the fatty acid amide hydrolase (FAAH), which results in accumulation of anandamide that possesses high affinity to CNR1 and CNR2 [62–64]. CBD might also act as an allosteric modulator of CNR1 and CNR2 [65–68]. Similarly, CBG can effectively regulate the endocannabinoid signaling via acting as a partial agonist of CNR2 or modulating CNR1 signaling, although the underlying mechanisms of the latter are unclear [27]. The mechanisms whereby CBD or CBG might modulate the homeostasis of bone cells or chondrocytes *in vivo* are uninvestigated. Our data unraveled striking similarities between CBD and CBG in promoting both early and late phases of bone healing. During the inflammatory phase, both CBD and CBG increased the abundance of the PDGFRα$^+$ progenitors in the healing hematoma (Fig. 9A), which might be the outcome of increasing the proliferation and/or the infiltration of these progenitors in the fracture callus. CBD and CBG also directly promoted the osteogenic differentiation of primary PDGFRα$^+$ progenitors *in vitro* (Fig. 9B). As healing proceeded to the repair phase, CBD and CBG enhanced the expression of the osteogenic proteins Col I, OC, and SP7 in the chondrocytes (Fig. 3A, D, E). These proteins are essential for the mineralization of the soft callus and for endochondral bone formation. Both CBD and CBG inhibited the apoptosis and enhanced the proliferation of bone and BM cells (Fig. 4–7). Accordingly, CBD and CBG exhibited protective and proliferative effects on several types of cells that play central roles during different phases of healing. The plasma concentrations that we detected after injecting 5 mg/kg/day (i.p.) of either CBD or CBG for 3 or 4 weeks were ~100–150 ng/ml (Fig. 1E). The reported plasma concentration of CBD in patients, following administration of 20 mg/kg/day for 22 days, is 400 ng/ml (i.e, ~1.2 μM) [69]. Therefore, the therapeutic effects of CBD that we observed in this study can be achieved without exceeding the clinically approved dose [69]. A previous study investigated the effect of CBD alone or in combination with the psychoactive cannabis constituent Δ^9-tetrahydrocannabinol (THC) on fracture healing using a rat model of femur fracture [25]. The study reported that CBD, but not THC, enhanced the biomechanical properties of healed bone as indicated by an increase in the maximal load and work-to-failure, but not stiffness [25], which is consistent with our data. However, the study did not detect any significant increase in the callus material density as a result of CBD and/or THC treatment [25]. More pre-clinical studies are required to investigate the therapeutic effects of CBD and CBG in other fracture models, and future clinical studies are also required to assess the effects of CBD and CBG in fracture patients. Notably, previous studies reported that CNR2 agonists can reduce breast cancer-induced bone loss and pain[70], providing further evidence for the wide therapeutic potential of cannabinoids as well as modulators of cannabinoid receptors in bone diseases.

We performed the *in-vitro* osteogenic differentiation of the PDGFRα$^+$ progenitors in the presence of 1 μM of CBD Fig. 9B), a concentration that was chosen to be comparable to the clinically reported plasma level of CBD [69]. In fact, when we used > 10 μM of either CBD or CBG in these *in-vitro* differentiation experiments, we observed significant apoptosis, and when the concentration of either drug exceeded 50 μM, most of the cells died within 24–48 h (data not shown). These data show how the outcome of *in-vitro* experiments might change

drastically based on the concentration for each cannabinoid. Accordingly, upon designing *in-vitro* studies, it is advisable to use cannabinoid concentrations that are relevant to the endogenous conditions.

Overall, the protective, proliferative, and pro-osteogenic effects that we identified for CBD and CBG during the different healing phases culminated in accelerated repair, promoted bone formation, and enhanced biomechanical strength of the healed bone. These data extend our understanding of the impact of CBD on fracture healing and demonstrate for the first time the therapeutic potential of CBG in the context of bone regeneration and repair. Taken together, the data we present here propose CBD and CBG as effective alternatives to the NSAIDs in managing pain in fracture patients.

Supplementary Material

Refer to Web version on PubMed Central for supplementary material.

Acknowledgments

Analysis of the plasma concentrations of CBD and CBG was performed at the Mass Spectrometry Core Facility (small molecules) (RRID # is SCR_017831), and the FC analysis was performed at the Flow Cytometry and Cell Sorting core (RRID # SCR_021134) at the Penn State University College of Medicine. KEV (and the Penn State College of Medicine) is the recipient of research support from PA Options for Wellness (a state-approved medical marijuana clinical registrant). The funding sources were not involved in study design, providing any experimental materials, data collection, data analysis and interpretation, writing of the report, or the decision to submit the article for publication. The authors would like to acknowledge members of the state-approved medical marijuana academic clinical research center at Penn State for insights and comments on the data and study design. This work was supported by the National Institutes of Health (NIH) R01 DK121327 to R.A.E. and R01 AR071968 to F.K.

References

1. Claes L, Recknagel S, Ignatius A. Fracture healing under healthy and inflammatory conditions. Nat Rev Rheumatol. Jan 31 2012;8(3):133–43. Epub 2012/02/02. [PubMed: 22293759]
2. Khajuria DK, Soliman M, Elfar JC, Lewis GS, Abraham T, Kamal F, et al. Aberrant structure of fibrillar collagen and elevated levels of advanced glycation end products typify delayed fracture healing in the diet-induced obesity mouse model. Bone. Aug 2020;137:115436. Epub 2020/05/23.
3. Baht GS, Vi L, Alman BA. The Role of the Immune Cells in Fracture Healing. Curr Osteoporos Rep. Apr 2018;16(2):138–45. Epub 2018/03/07. [PubMed: 29508143]
4. Giannoudis PV, MacDonald DA, Matthews SJ, Smith RM, Furlong AJ, De Boer P. Nonunion of the femoral diaphysis. The influence of reaming and non-steroidal anti-inflammatory drugs. J Bone Joint Surg Br. Jul 2000;82(5):655–8. Epub 2000/08/30. [PubMed: 10963160]
5. O'Connor JP, Capo JT, Tan V, Cottrell JA, Manigrasso MB, Bontempo N, et al. A comparison of the effects of ibuprofen and rofecoxib on rabbit fibula osteotomy healing. Acta Orthop. Oct 2009;80(5):597–605. Epub 2009/11/18. [PubMed: 19916696]
6. Simon AM, O'Connor JP. Dose and time-dependent effects of cyclooxygenase-2 inhibition on fracture-healing. J Bone Joint Surg Am. Mar 2007;89(3):500–11. Epub 2007/03/03. [PubMed: 17332098]
7. Simon AM, Manigrasso MB, O'Connor JP. Cyclo-oxygenase 2 function is essential for bone fracture healing. J Bone Miner Res. Jun 2002;17(6):963–76. Epub 2002/06/11. [PubMed: 12054171]
8. Gerstenfeld LC, Thiede M, Seibert K, Mielke C, Phippard D, Svagr B, et al. Differential inhibition of fracture healing by non-selective and cyclooxygenase-2 selective non-steroidal anti-inflammatory drugs. J Orthop Res. Jul 2003;21(4):670–5. Epub 2003/06/12. [PubMed: 12798067]

9. Murnaghan M, Li G, Marsh DR. Nonsteroidal anti-inflammatory drug-induced fracture nonunion: an inhibition of angiogenesis? J Bone Joint Surg Am. Nov 2006;88 Suppl 3:140–7. Epub 2006/11/03. [PubMed: 17079380]
10. Bhattacharyya T, Levin R, Vrahas MS, Solomon DH. Nonsteroidal antiinflammatory drugs and nonunion of humeral shaft fractures. Arthritis Rheum. Jun 15 2005;53(3):364–7. Epub 2005/06/04. [PubMed: 15934108]
11. Chau DL, Walker V, Pai L, Cho LM. Opiates and elderly: use and side effects. Clin Interv Aging. 2008;3(2):273–8. Epub 2008/08/09. [PubMed: 18686750]
12. Kidner CL, Mayer TG, Gatchel RJ. Higher opioid doses predict poorer functional outcome in patients with chronic disabling occupational musculoskeletal disorders. J Bone Joint Surg Am. Apr 2009;91(4):919–27. Epub 2009/04/03. [PubMed: 19339577]
13. Sullivan MD, Howe CQ. Opioid therapy for chronic pain in the United States: promises and perils. Pain. Dec 2013;154 Suppl 1:S94–S100. Epub 2013/09/17. [PubMed: 24036286]
14. Jain N, Himed K, Toth JM, Briley KC, Phillips FM, Khan SN. Opioids delay healing of spinal fusion: a rabbit posterolateral lumbar fusion model. Spine J. Sep 2018;18(9):1659–68. Epub 2018/04/24. [PubMed: 29680509]
15. McVeigh LG, Perugini AJ, Fehrenbacher JC, White FA, Kacena MA. Assessment, Quantification, and Management of Fracture Pain: from Animals to the Clinic. Curr Osteoporos Rep. Oct 2020;18(5):460–70. Epub 2020/08/23. [PubMed: 32827293]
16. Mitchell SAT, Majuta LA, Mantyh PW. New Insights in Understanding and Treating Bone Fracture Pain. Curr Osteoporos Rep. Aug 2018;16(4):325–32. Epub 2018/06/28. [PubMed: 29948820]
17. Mantyh PW. The neurobiology of skeletal pain. Eur J Neurosci. Feb 2014;39(3):508–19. Epub 2014/02/06. [PubMed: 24494689]
18. Alves CJ, Neto E, Sousa DM, Leitao L, Vasconcelos DM, Ribeiro-Silva M, et al. Fracture pain-Traveling unknown pathways. Bone. Apr 2016;85:107–14. Epub 2016/02/07. [PubMed: 26851411]
19. Feinberg SD. Prescribing analgesics. How to improve function and avoid toxicity when treating chronic pain. Geriatrics. Nov 2000;55(11):44, 9–50, 3 passim. Epub 2000/11/22.
20. Koester MC, Spindler KP. NSAIDs and fracture healing: what's the evidence? Curr Sports Med Rep. Dec 2005;4(6):289–90. Epub 2005/11/12. [PubMed: 16282028]
21. Koester MC, Spindler KP. Pharmacologic agents in fracture healing. Clin Sports Med. Jan 2006;25(1):63–73, viii. Epub 2005/12/06. [PubMed: 16324974]
22. Wheeler P, Batt ME. Do non-steroidal anti-inflammatory drugs adversely affect stress fracture healing? A short review. Br J Sports Med. Feb 2005;39(2):65–9. Epub 2005/01/25. [PubMed: 15665197]
23. Hsu WY, Lin CL, Kao CH. Association between opioid use disorder and fractures: a population-based study. Addiction. Nov 2019;114(11):2008–15. Epub 2019/07/16. [PubMed: 31307110]
24. Legare CA, Raup-Konsavage WM, Vrana KE. Therapeutic Potential of Cannabis, Cannabidiol, and Cannabinoid-Based Pharmaceuticals. Pharmacology. 2022;107(3–4):131–49. Epub 2022/01/31. [PubMed: 35093949]
25. Kogan NM, Melamed E, Wasserman E, Raphael B, Breuer A, Stok KS, et al. Cannabidiol, a Major Non-Psychotropic Cannabis Constituent Enhances Fracture Healing and Stimulates Lysyl Hydroxylase Activity in Osteoblasts. J Bone Miner Res. Oct 2015;30(10):1905–13. Epub 2015/03/25. [PubMed: 25801536]
26. Li D, Lin Z, Meng Q, Wang K, Wu J, Yan H. Cannabidiol administration reduces sublesional cancellous bone loss in rats with severe spinal cord injury. Eur J Pharmacol. Aug 15 2017;809:13–9. Epub 2017/05/10. [PubMed: 28479140]
27. Navarro G, Varani K, Reyes-Resina I, Sanchez de Medina V, Rivas-Santisteban R, Sanchez-Carnerero Callado C, et al. Cannabigerol Action at Cannabinoid CB1 and CB2 Receptors and at CB1-CB2 Heteroreceptor Complexes. Front Pharmacol. 2018;9:632. Epub 2018/07/07. [PubMed: 29977202]
28. Brown ML, Yukata K, Farnsworth CW, Chen DG, Awad H, Hilton MJ, et al. Delayed fracture healing and increased callus adiposity in a C57BL/6J murine model of obesity-associated type 2 diabetes mellitus. PLoS One. 2014;9(6):e99656. Epub 2014/06/10. [PubMed: 24911161]

29. Khajuria DK, Nowak I, Leung M, Karuppagounder V, Imamura Y, Norbury CC, et al. Transcript shortening via alternative polyadenylation promotes gene expression during fracture healing. Bone Res. Jan 3 2023;11(1):5. Epub 2023/01/04. [PubMed: 36596777]
30. Hogevold HE, Grogaard B, Reikeras O. Effects of short-term treatment with corticosteroids and indomethacin on bone healing. A mechanical study of osteotomies in rats. Acta Orthop Scand. Dec 1992;63(6):607–11. Epub 1992/12/01. [PubMed: 1471505]
31. Bergenstock M, Min W, Simon AM, Sabatino C, O'Connor JP. A comparison between the effects of acetaminophen and celecoxib on bone fracture healing in rats. J Orthop Trauma. Nov-Dec 2005;19(10):717–23. Epub 2005/11/30. [PubMed: 16314720]
32. Kogan NM, Lavi Y, Topping LM, Williams RO, McCann FE, Yekhtin Z, et al. Novel CBG Derivatives Can Reduce Inflammation, Pain and Obesity. Molecules. Sep 15 2021;26(18). Epub 2021/09/29.
33. Rock EM, Goodwin JM, Limebeer CL, Breuer A, Pertwee RG, Mechoulam R, et al. Interaction between non-psychotropic cannabinoids in marihuana: effect of cannabigerol (CBG) on the anti-nausea or anti-emetic effects of cannabidiol (CBD) in rats and shrews. Psychopharmacology (Berl). Jun 2011;215(3):505–12. Epub 2011/01/19. [PubMed: 21243485]
34. Xu J, Wang Y, Li Z, Tian Y, Li Z, Lu A, et al. PDGFRalpha reporter activity identifies periosteal progenitor cells critical for bone formation and fracture repair. Bone Res. Jan 25 2022;10(1):7. Epub 2022/01/26. [PubMed: 35075130]
35. Sepulveda DE, Morris DP, Raup-Konsavage WM, Sun D, Vrana KE, Graziane NM. Cannabigerol (CBG) attenuates mechanical hypersensitivity elicited by chemotherapy-induced peripheral neuropathy. Eur J Pain. Oct 2022;26(9):1950–66. Epub 2022/07/29. [PubMed: 35899583]
36. Karuppagounder V, Chung J, Abdeen A, Thompson A, Bouboukas A, Pinamont WJ, et al. Distinctive Therapeutic Effects of Non-Euphorigenic Cannabis Extracts in Osteoarthritis. Cannabis Cannabinoid Res. Aug 22 2022. Epub 2022/08/23.
37. Minville V, Laffosse JM, Fourcade O, Girolami JP, Tack I. Mouse model of fracture pain. Anesthesiology. Mar 2008;108(3):467–72. Epub 2008/02/23. [PubMed: 18292684]
38. Pinamont WJ, Yoshioka NK, Young GM, Karuppagounder V, Carlson EL, Ahmad A, et al. Standardized Histomorphometric Evaluation of Osteoarthritis in a Surgical Mouse Model. J Vis Exp. May 6 2020(159). Epub 2020/05/26.
39. Kegelman CD, Nijsure MP, Moharrer Y, Pearson HB, Dawahare JH, Jordan KM, et al. YAP and TAZ Promote Periosteal Osteoblast Precursor Expansion and Differentiation for Fracture Repair. J Bone Miner Res. Jan 2021;36(1):143–57. Epub 2020/08/25. [PubMed: 32835424]
40. Nakamichi Y, Udagawa N, Horibe K, Mizoguchi T, Yamamoto Y, Nakamura T, et al. VDR in Osteoblast-Lineage Cells Primarily Mediates Vitamin D Treatment-Induced Increase in Bone Mass by Suppressing Bone Resorption. J Bone Miner Res. Jun 2017;32(6):1297–308. Epub 2017/02/09. [PubMed: 28177161]
41. Carlson EL, Karuppagounder V, Pinamont WJ, Yoshioka NK, Ahmad A, Schott EM, et al. Paroxetine-mediated GRK2 inhibition is a disease-modifying treatment for osteoarthritis. Sci Transl Med. Feb 10 2021;13(580). Epub 2021/02/12.
42. Yoshioka NK, Young GM, Khajuria DK, Karuppagounder V, Pinamont WJ, Fanburg-Smith JC, et al. Structural changes in the collagen network of joint tissues in late stages of murine OA. Sci Rep. Jun 1 2022;12(1):9159. Epub 2022/06/02. [PubMed: 35650306]
43. Karuppagounder V, Pinamont W, Yoshioka N, Elbarbary R, Kamal F. Early Gbetagamma-GRK2 Inhibition Ameliorates Osteoarthritis Development by Simultaneous Anti-Inflammatory and Chondroprotective Effects. Int J Mol Sci. Jul 19 2022;23(14). Epub 2022/07/28.
44. Wee H, Khajuria DK, Kamal F, Lewis GS, Elbarbary RA. Assessment of Bone Fracture Healing Using Micro-Computed Tomography. J Vis Exp. Dec 9 2022(190). Epub 2022/12/27.
45. Ortuno MJ, Susperregui AR, Artigas N, Rosa JL, Ventura F. Osterix induces Col1a1 gene expression through binding to Sp1 sites in the bone enhancer and proximal promoter regions. Bone. Feb 2013;52(2):548–56. Epub 2012/11/20. [PubMed: 23159876]
46. Matsubara T, Kida K, Yamaguchi A, Hata K, Ichida F, Meguro H, et al. BMP2 regulates Osterix through Msx2 and Runx2 during osteoblast differentiation. J Biol Chem. Oct 24 2008;283(43):29119–25. Epub 2008/08/16. [PubMed: 18703512]

47. Xing W, Godwin C, Pourteymoor S, Mohan S. Conditional disruption of the osterix gene in chondrocytes during early postnatal growth impairs secondary ossification in the mouse tibial epiphysis. Bone Res. 2019;7:24. Epub 2019/10/28. [PubMed: 31646014]
48. Xiong W, Cui T, Cheng K, Yang F, Chen SR, Willenbring D, et al. Cannabinoids suppress inflammatory and neuropathic pain by targeting alpha3 glycine receptors. J Exp Med. Jun 4 2012;209(6):1121–34. Epub 2012/05/16. [PubMed: 22585736]
49. Nichols JM, Kaplan BLF. Immune Responses Regulated by Cannabidiol. Cannabis Cannabinoid Res. Mar 1 2020;5(1):12–31. Epub 2020/04/24. [PubMed: 32322673]
50. Henriquez JE, Rizzo MD, Schulz MA, Crawford RB, Gulick P, Kaminski NE. Delta9-Tetrahydrocannabinol Suppresses Secretion of IFNalpha by Plasmacytoid Dendritic Cells From Healthy and HIV-Infected Individuals. J Acquir Immune Defic Syndr. Aug 15 2017;75(5):588–96. Epub 2017/07/12. [PubMed: 28692581]
51. Carrillo-Salinas FJ, Navarrete C, Mecha M, Feliu A, Collado JA, Cantarero I, et al. A cannabigerol derivative suppresses immune responses and protects mice from experimental autoimmune encephalomyelitis. PLoS One. 2014;9(4):e94733. Epub 2014/04/15. [PubMed: 24727978]
52. Ofek O, Karsak M, Leclerc N, Fogel M, Frenkel B, Wright K, et al. Peripheral cannabinoid receptor, CB2, regulates bone mass. Proc Natl Acad Sci U S A. Jan 17 2006;103(3):696–701. Epub 2006/01/13. [PubMed: 16407142]
53. Idris AI, van 't Hof RJ, Greig IR, Ridge SA, Baker D, Ross RA, et al. Regulation of bone mass, bone loss and osteoclast activity by cannabinoid receptors. Nat Med. Jul 2005;11(7):774–9. Epub 2005/05/24. [PubMed: 15908955]
54. Tam J, Trembovler V, Di Marzo V, Petrosino S, Leo G, Alexandrovich A, et al. The cannabinoid CB1 receptor regulates bone formation by modulating adrenergic signaling. FASEB J. Jan 2008;22(1):285–94. Epub 2007/08/21. [PubMed: 17704191]
55. Tam J, Ofek O, Fride E, Ledent C, Gabet Y, Muller R, et al. Involvement of neuronal cannabinoid receptor CB1 in regulation of bone mass and bone remodeling. Mol Pharmacol. Sep 2006;70(3):786–92. Epub 2006/06/15. [PubMed: 16772520]
56. Ofek O, Attar-Namdar M, Kram V, Dvir-Ginzberg M, Mechoulam R, Zimmer A, et al. CB2 cannabinoid receptor targets mitogenic Gi protein-cyclin D1 axis in osteoblasts. J Bone Miner Res. Feb 2011;26(2):308–16. Epub 2010/08/31. [PubMed: 20803555]
57. Matsuda LA, Lolait SJ, Brownstein MJ, Young AC, Bonner TI. Structure of a cannabinoid receptor and functional expression of the cloned cDNA. Nature. Aug 9 1990;346(6284):561–4. Epub 1990/08/09. [PubMed: 2165569]
58. Munro S, Thomas KL, Abu-Shaar M. Molecular characterization of a peripheral receptor for cannabinoids. Nature. Sep 2 1993;365(6441):61–5. Epub 1993/09/02. [PubMed: 7689702]
59. Kaplan BL, Springs AE, Kaminski NE. The profile of immune modulation by cannabidiol (CBD) involves deregulation of nuclear factor of activated T cells (NFAT). Biochem Pharmacol. Sep 15 2008;76(6):726–37. Epub 2008/07/29. [PubMed: 18656454]
60. Thapa D, Cairns EA, Szczesniak AM, Toguri JT, Caldwell MD, Kelly MEM. The Cannabinoids Delta(8)THC, CBD, and HU-308 Act via Distinct Receptors to Reduce Corneal Pain and Inflammation. Cannabis Cannabinoid Res. 2018;3(1):11–20. Epub 2018/02/17. [PubMed: 29450258]
61. Khuja I, Yekhtin Z, Or R, Almogi-Hazan O. Cannabinoids Reduce Inflammation but Inhibit Lymphocyte Recovery in Murine Models of Bone Marrow Transplantation. Int J Mol Sci. Feb 4 2019;20(3). Epub 2019/02/06.
62. de Filippis D, Iuvone T, d'amico A, Esposito G, Steardo L, Herman AG, et al. Effect of cannabidiol on sepsis-induced motility disturbances in mice: involvement of CB receptors and fatty acid amide hydrolase. Neurogastroenterol Motil. Aug 2008;20(8):919–27. Epub 2008/04/01. [PubMed: 18373655]
63. Pazos MR, Mohammed N, Lafuente H, Santos M, Martinez-Pinilla E, Moreno E, et al. Mechanisms of cannabidiol neuroprotection in hypoxic-ischemic newborn pigs: role of 5HT(1A) and CB2 receptors. Neuropharmacology. Aug 2013;71:282–91. Epub 2013/04/17. [PubMed: 23587650]

64. Facci L, Dal Toso R, Romanello S, Buriani A, Skaper SD, Leon A. Mast cells express a peripheral cannabinoid receptor with differential sensitivity to anandamide and palmitoylethanolamide. Proc Natl Acad Sci U S A. Apr 11 1995;92(8):3376–80. Epub 1995/04/11. [PubMed: 7724569]

65. Laprairie RB, Bagher AM, Kelly ME, Denovan-Wright EM. Cannabidiol is a negative allosteric modulator of the cannabinoid CB1 receptor. Br J Pharmacol. Oct 2015;172(20):4790–805. Epub 2015/07/29. [PubMed: 26218440]

66. Tham M, Yilmaz O, Alaverdashvili M, Kelly MEM, Denovan-Wright EM, Laprairie RB. Allosteric and orthosteric pharmacology of cannabidiol and cannabidiol-dimethylheptyl at the type 1 and type 2 cannabinoid receptors. Br J Pharmacol. May 2019;176(10):1455–69. Epub 2018/07/08. [PubMed: 29981240]

67. Navarro G, Reyes-Resina I, Rivas-Santisteban R, Sanchez de Medina V, Morales P, Casano S, et al. Cannabidiol skews biased agonism at cannabinoid CB1 and CB2 receptors with smaller effect in CB1-CB2 heteroreceptor complexes. Biochem Pharmacol. Nov 2018;157:148–58. Epub 2018/09/09. [PubMed: 30194918]

68. Martinez-Pinilla E, Varani K, Reyes-Resina I, Angelats E, Vincenzi F, Ferreiro-Vera C, et al. Binding and Signaling Studies Disclose a Potential Allosteric Site for Cannabidiol in Cannabinoid CB2 Receptors. Front Pharmacol. 2017;8:744. Epub 2017/11/08. [PubMed: 29109685]

69. Devinsky O, Patel AD, Thiele EA, Wong MH, Appleton R, Harden CL, et al. Randomized, dose-ranging safety trial of cannabidiol in Dravet syndrome. Neurology. Apr 3 2018;90(14):e1204–e11. Epub 2018/03/16. [PubMed: 29540584]

70. Lozano-Ondoua AN, Hanlon KE, Symons-Liguori AM, Largent-Milnes TM, Havelin JJ, Ferland HL 3rd, et al. Disease modification of breast cancer-induced bone remodeling by cannabinoid 2 receptor agonists. J Bone Miner Res. Jan 2013;28(1):92–107. Epub 2012/08/21. [PubMed: 22903605]

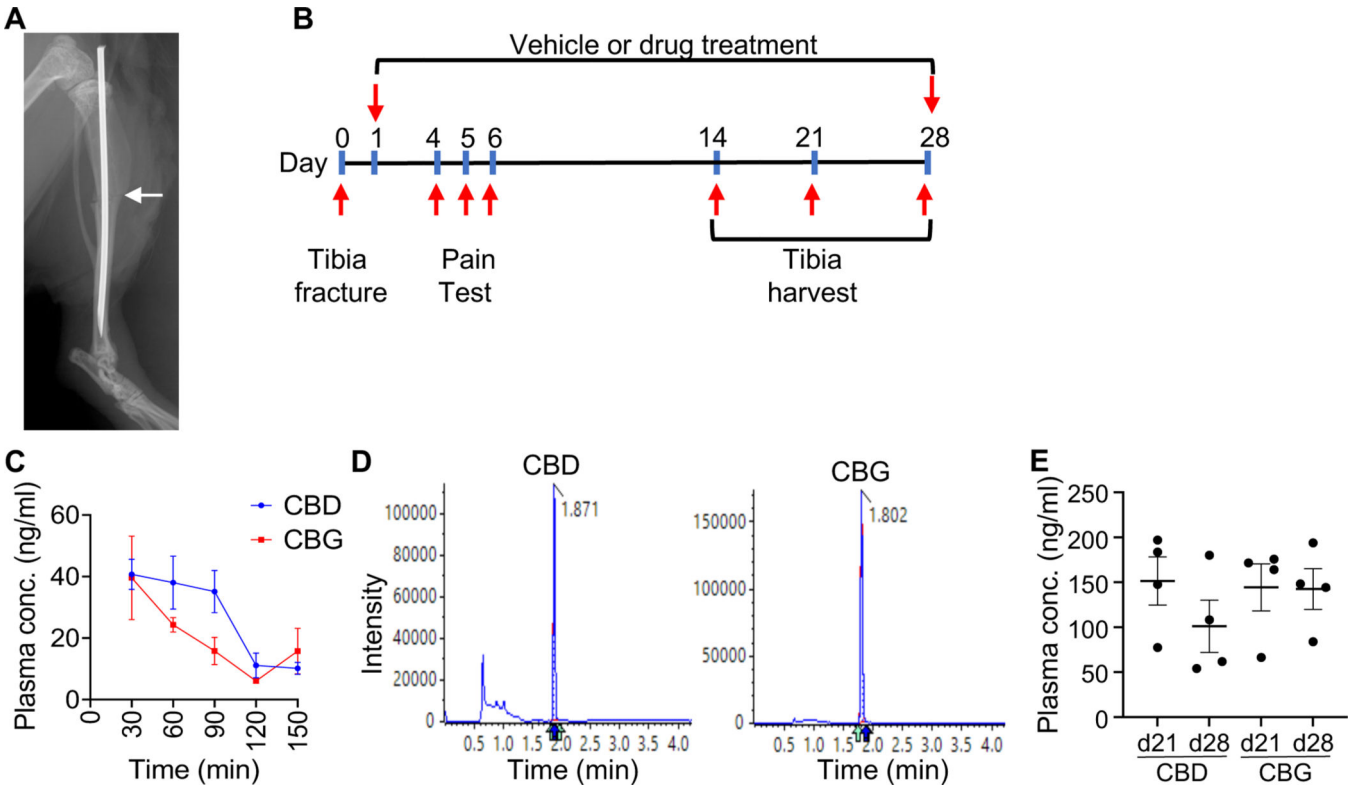

Figure 1. Measuring the plasma concentration of CBD and CBG following acute and chronic administration.

(A) An X-ray image captured post-operatively. The image shows the fracture line (white arrow) and the intramedullary nail that was used to stabilize the fracture. **(B)** A schematic of the experimental timeline. **(C)** The plasma concentrations (ng/ml) of CBD (blue) and CBG (red) measured at the indicated timepoints following administration of the first dose. The analysis was performed using liquid chromatography coupled with tandem mass spectrometry (LC-MS-MS). N = 4. The line presents average ± SEM. (**D**) Representative mass spectra that show the analysis of CBD (left) or CBG (right) in plasma samples. The retention time of each compound is indicated. (**E**) As in (C), except that the concentration of CBD and CBG were measured following daily administration of each drug for 21 or 28 days (d21 and d28 samples, respectively).

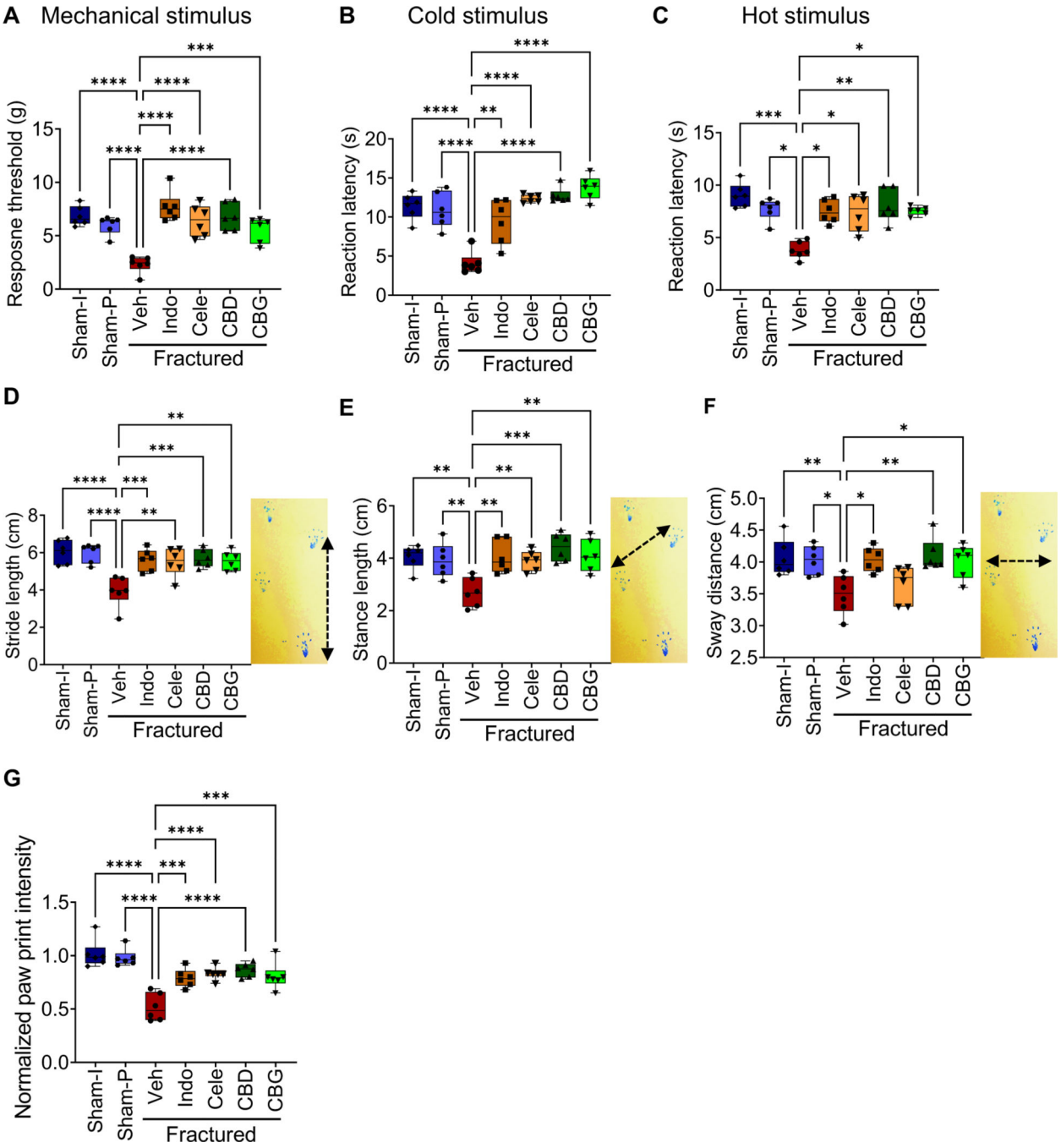

Figure 2. CBD and CBG ameliorate post-fracture pain as effectively as the NSAIDs.

(A-C) Tests for mechanical allodynia (**A**; von Frey test), sensitivity to cold stimulus (**B**; acetone drop test), and sensitivity to hot stimulus (**C**; hot plate test; the hot plate was adjusted at 52° C). Sham-I: control unfractured mice that underwent skin incision only. Sham-P: like Sham-I, except that a nail was inserted in the intramedullary cavity to mimic the nail used to stabilize the fracture gap in the fractured mice (Fig. 1A). These Sham-I mice were used to normalize for any effects that the intramedullary nail might have on the animal nociception. The fractured mice were treated with vehicle (Veh), indomethacin

(Indo), celecoxib (Cele), CBD, or CBG, while both the Sham-P and Sham-I groups were treated with Veh. All pain tests were performed on the fractured limb or the corresponding limb in the sham-operated mice. All tests were performed 1 h following administration of the indicated treatment. For the von Frey test, the threshold required to elicit a withdrawal response was recorded. For the acetone drop and hot plate tests, the time required to elicit a nociceptive behavior (paw withdrawal or paw licking) was recorded. The von Frey and acetone drop tests were performed three times on each mouse with an interval of 10 minutes. (**D-F**) Results of the Catwalk gait analysis measuring the stride length (**D**), stance length (**E**), or sway distance (**F**) in the indicated sham and treatment groups. The image next to each boxplot shows how the parameter was measured. (**G**) Catwalk gait analysis was used to measure the intensity of paw print of both the fractured and unfractured limbs in each mouse. The intensity of paw print of the fractured limb was normalized to that of the contralateral unfractured limb, and the normalized intensity in the Sham I mice was defined as 1.. All gait analyses (**D-G**) were performed three times for each mouse, and at least 10 steps were analyzed each time.

For all experiments, N = 6 mice. All box and whiskers plots are presented as min to max and line at median. (*) $P < 0.05$, (**) $P < 0.01$, (***) $P < 0.001$, and (****) $P < 0.0001$, using one-way analysis of variance (ANOVA) followed by Tukey’s post hoc test.

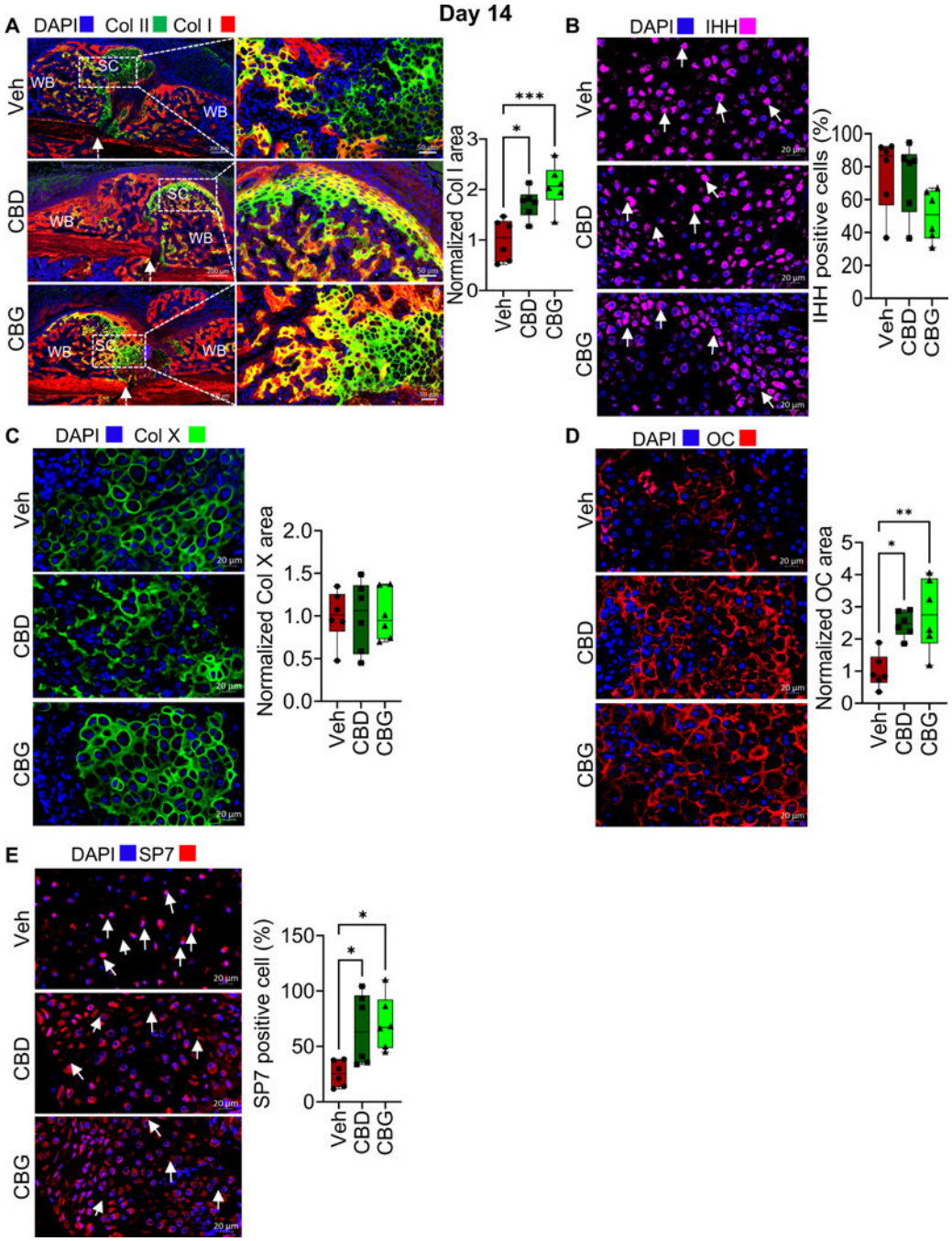

Figure 3. CBD and CBG promote the mineralization of the fibrocartilaginous callus.

(A, left) IF co-staining of Col I (red) and Col II (green) in the callus of d14. The calli were isolated from mice treated with vehicle (Veh), CBD, or CBG. DAPI (blue) stains nuclei. The scale bar = 200 μm. SC: soft callus (i.e., fibrocartilaginous callus). WB: woven bone. The white arrows point to the fracture line. Col II marks the chondrocytes in the SC, which fill the areas within and in close vicinity of the fracture gap. Col I marks the WB, which forms at callus areas distal to the fracture line (see also Fig. S1A, B). The regions where both Col I and Col II are expressed (yellow areas) surround Col I-expressing chondrocytes.

(A, middle) Magnified images of the SC areas that are indicated by the white boxes in (A, left). The scale bar = 50 μm. (**A, right**) Quantification of Col I staining/expression in the SC. The area of Col I staining was normalized to the area of the SC, and the normalized area in the Veh-treated mice was defined as 1 (see Materials and Methods). (**B, left**) IF staining of IHH (magenta) in the SC. DAPI (blue) stains nuclei. (**B, right**) Quantification of IHH staining. The number of IHH-positive chondrocytes was normalized to the total number of chondrocytes (defined by DAPI staining) in the SC, and the ratio was presented as % (see Materials and Methods).. (**C**) As in (**A**), except that Col X was stained (green) and quantified. (**D**) As in (**A**), except that OC was stained (red) and quantified in the SC. (**E**) As in (**B**), except that SP7 was stained (magenta) and quantified in the SC chondrocytes. IF images are representative of 6 mice. All box and whiskers plots are presented as min to max and line at median. (*) $P < 0.05$, (**) $P < 0.01$, (***) $P < 0.001$, and (****) $P < 0.0001$, using one-way ANOVA followed by Tukey's post hoc test.

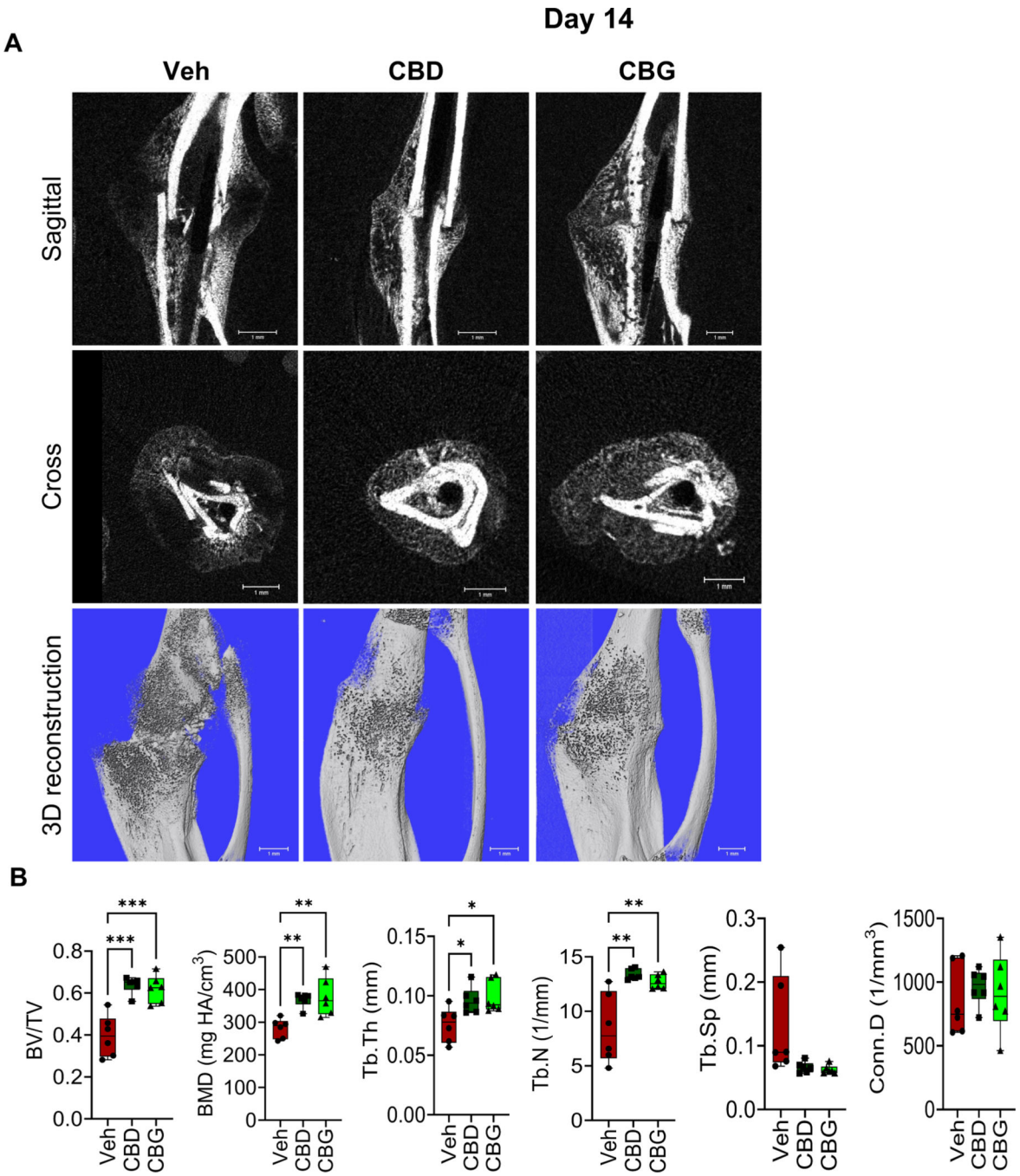

Figure 4. CBD and CBG enhance bone formation on d14 post-fracture.

(**A**) μCT images of the fractured right hindlimb captured on d14. (**B**) Results of μCT analysis of d14 callus in the specified treatment groups N = 6 mice. All box and whiskers plots are presented as min to max and line at median. (*) $P < 0.05$, (**) $P < 0.01$, using one-way ANOVA followed by Tukey's post hoc test.

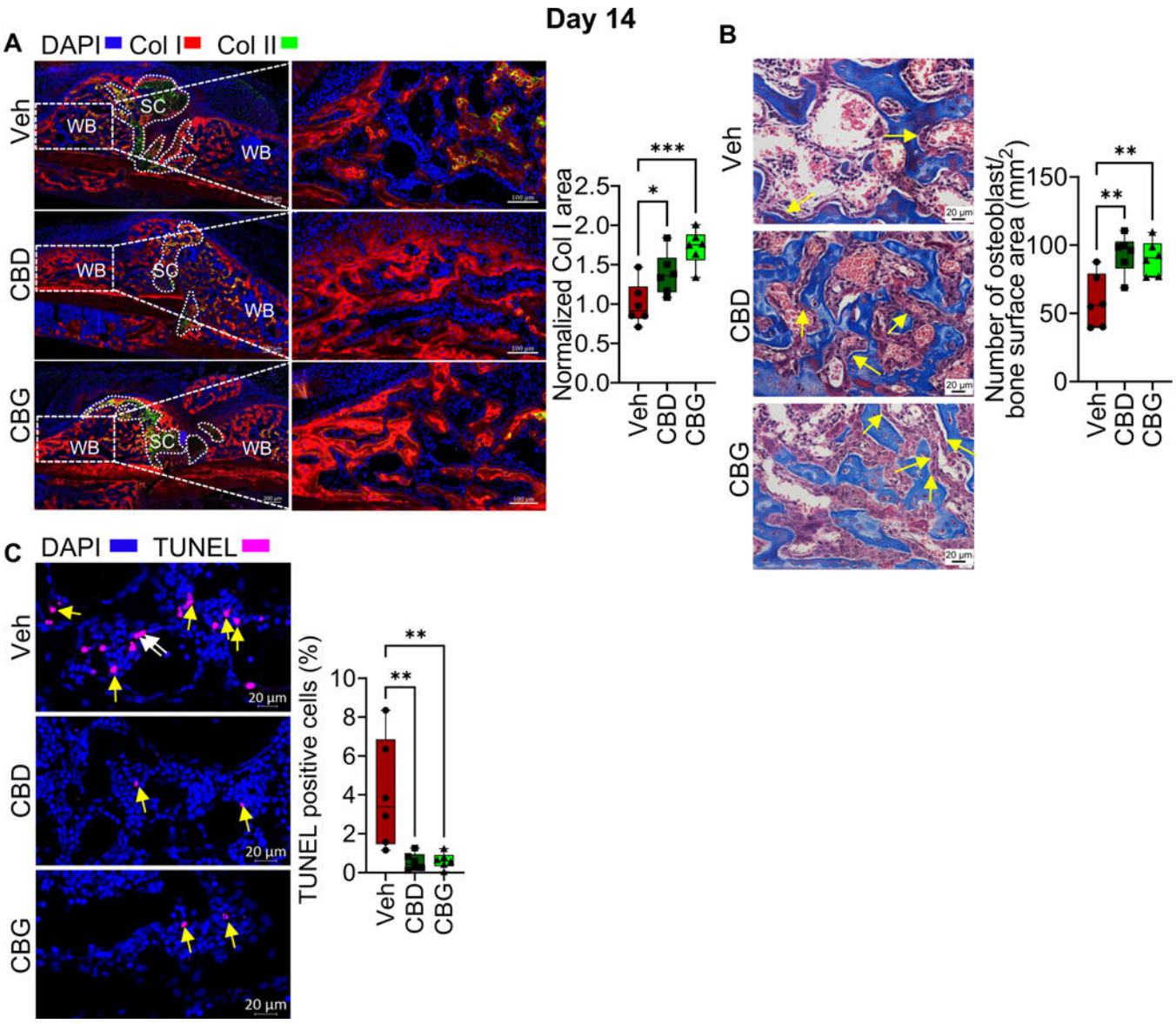

Figure 5. CBD and CBG enhance cell viability and promote Col I expression in the woven bone area of d14 callus.

(A, left) IF co-staining of Col I (red) and Col II (green) in the calli of d14. The calli were isolated from mice treated with vehicle (Veh), CBD, or CBG. DAPI (blue) stains nuclei. The scale bar = 200 μm. SC: soft callus. WB: woven bone. Col II marks the chondrocytes in the SC, which fill areas within and proximal to the fracture gap. Col I marks the WB, which forms at callus areas distal to the fracture line. **(A, middle)** Magnified images of the WB areas that are indicated by the white boxes in (A, left). The scale bar = 100 μm. **(A, right)** Quantification of Col I staining (i. e. expression) in the WB region. The Col I-stained area was normalized to the WB area, and the normalized area in the Veh-treated group was defined as 1. (**B, left**) Masson's trichome staining. Images were captured in the WB. The yellow arrows point to osteoblasts. The scale bar = 20 μm. (**B, right**) Quantification of the number of osteoblasts normalized to bone surface area. (**C, left**) TUNEL staining assay of

apoptotic cells (magenta) in the WB area. DAPI (blue) stains nuclei. The scale bar = 20 μm. The white arrows point to $TUNEL^+$ bone cells, and the yellow arrows point to $TUNEL^+$ BM cells. (**C, right**) Quantification of $TUNEL^+$ cells. The total number of $TUNEL^+$ cells (cells on bone surface + BM cells) was quantified and normalized to the total number of cells (defined by DAPI staining) in the WB area, and the ratio was presented as %.
For all Experiments, N = 6 mice. All box and whiskers plots are presented as min to max and line at median. (*) $P < 0.05$, (**) $P < 0.01$, and (***) $P < 0.001$, using one-way ANOVA followed by Tukey's post hoc test.

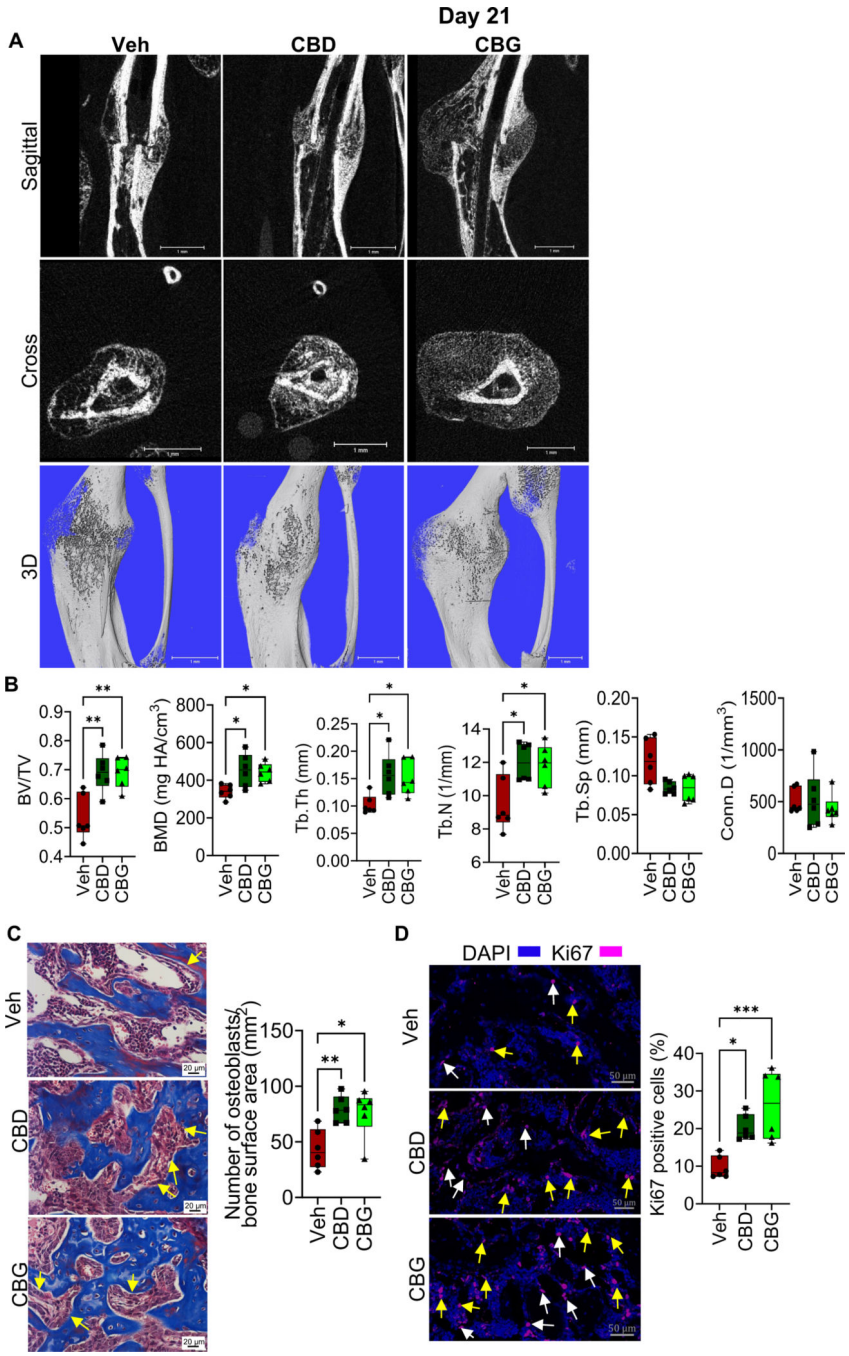

Figure 6. CBD and CBG accelerate the bony bridging of the fracture gap.

(A) μCT images of the fractured right hindlimb captured on d21. (**B**) Results of μCT analysis of d21 callus in the specified treatment groups (**C, left**) Masson's trichome staining of the d21 callus. The yellow arrows point to osteoblasts. The scale bar = 20 μm. (**C, right**) Quantification of the number of osteoblasts normalized to bone surface area. (**D, left**) IF staining of the proliferation marker Ki67 (magenta) in the d21 callus. The white arrows point to bone cells, and the yellow arrows point to BM cells. The scale bar = 50 μm. (**D, right**) Quantification of Ki67 staining. The total number of $Ki67^+$ cells (bone cells + BM

cells) was normalized to the total number of callus cells (defined by DAPI), and the ratio was presented as %.

For all Experiments, N = 6 mice. All box and whiskers plots are presented as min to max and line at median. (*) $P < 0.05$, (**) $P < 0.01$, and (***) $P < 0.001$ using one-way ANOVA followed by Tukey's post hoc test.

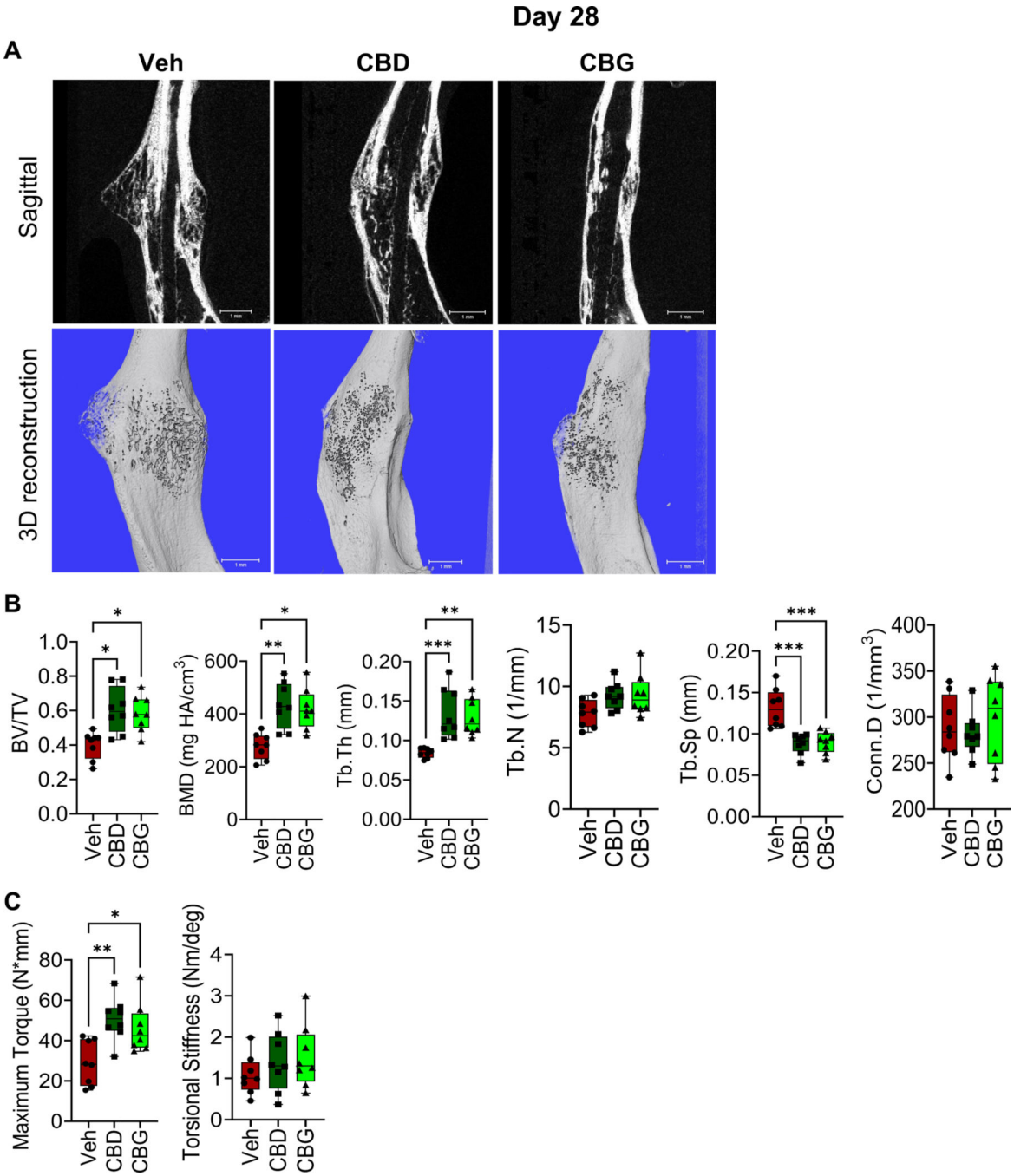

Figure 7. CBD or CBG treatment enhances the biomechanical properties of the newly formed bone.

(A) μCT images of the fractured right hindlimb captured on d28. (**B**) Results of μCT analysis of d28 callus in the specified treatment groups (**C**) Biomechanical testing on d28. For all tests, N=8. All box and whiskers plots are presented as min to max and line at median. (*) $P < 0.05$, (**) $P < 0.01$, using one-way ANOVA followed by Tukey's post hoc test.

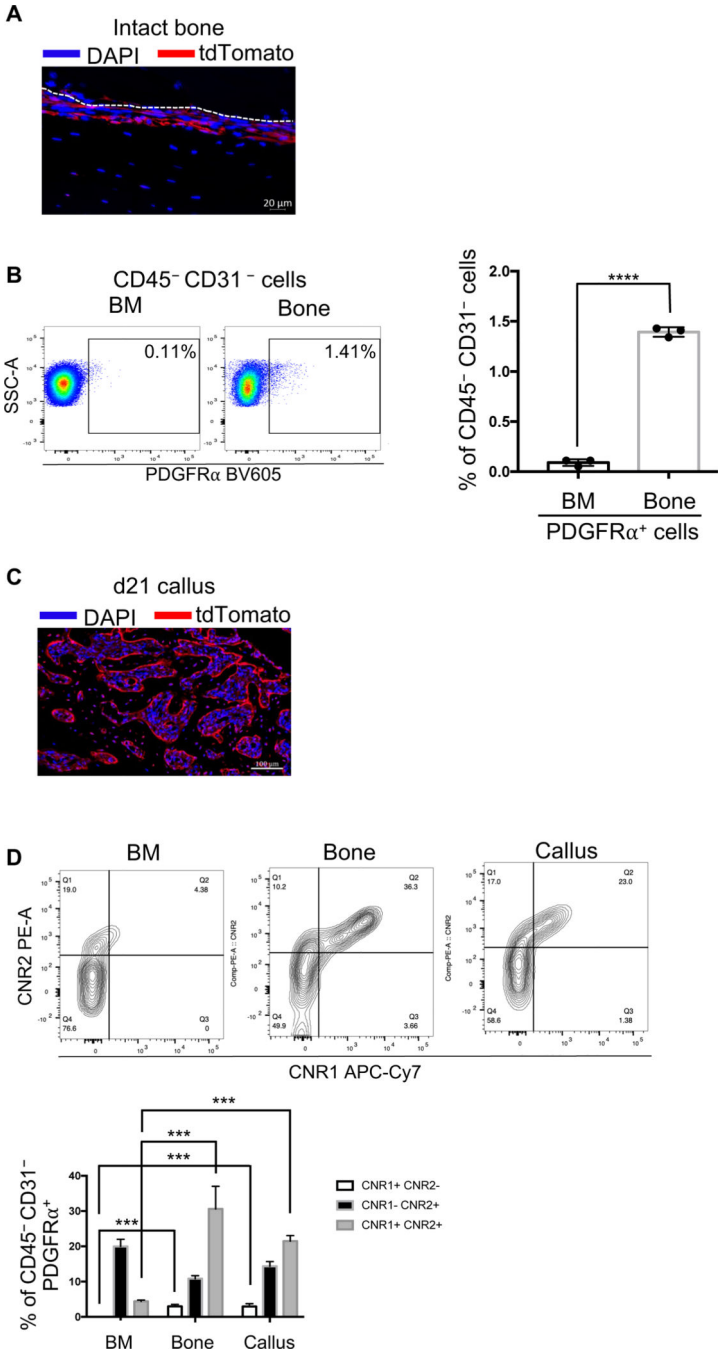

Figure 8. Differential expression of CNR1 and CNR2 in subpopulations of the PDGFRα$^+$ progenitors.

(**A**) The PDGFRα^{Ai9} mice were injected with 100 mg/kg of tamoxifen for 5 consecutive days. The intact bone was then harvested, and IF microscopy was used to detect the tdTomato reporter activity (red). DAPI (blue) stains nuclei. The scale bar = 20 μm. (**B, left**) A representative dot plot of the FC results, showing the abundance of PDGFRα$^+$ progenitors (i.e., CD45$^-$CD31$^-$ PDGFRα$^+$ cells) in the BM and intact bone. The % of PDGFRα$^+$ cells relative to the CD45$^-$CD31$^-$ (nonhematopoietic and nonendothelial) population in each

tissue is shown. (**B, right**) Quantification of the relative proportion of PDGFRα^{+} progenitors in the BM vs intact bone. (**C**) The PDGFRα^{Ai9} mice were injected with tamoxifen as in (A), fractured, and the fracture callus was harvested on d21 post-fracture. IF microscopy was used to detect the tdTomato reporter activity (red) in the callus. DAPI (blue) stains nuclei. The scale bar = 100 μm. (**D**, **top**) As in (B), except that the expression of CNR1 and CNR2 in the PDGFRα^{+} progenitors (CD45^{-}CD31^{-} PDGFRα^{+}) was analyzed. (**D, bottom**) As in (B, right), except that the proportion (%) of each of the indicated subpopulations of the PDGFRα^{+} progenitors was quantified.

The IF images are representative of N = 3. For FC analysis, N = 3, and 4 calli were pooled in each. The bar graphs present average ± SEM. (***) $P < 0.001$, (****) $P < 0.0001$. Student's *t* test was used in (B), and one-way ANOVA (followed by Tukey's post hoc test) was used in (D) to compare the abundance of each population among the 3 tissues.

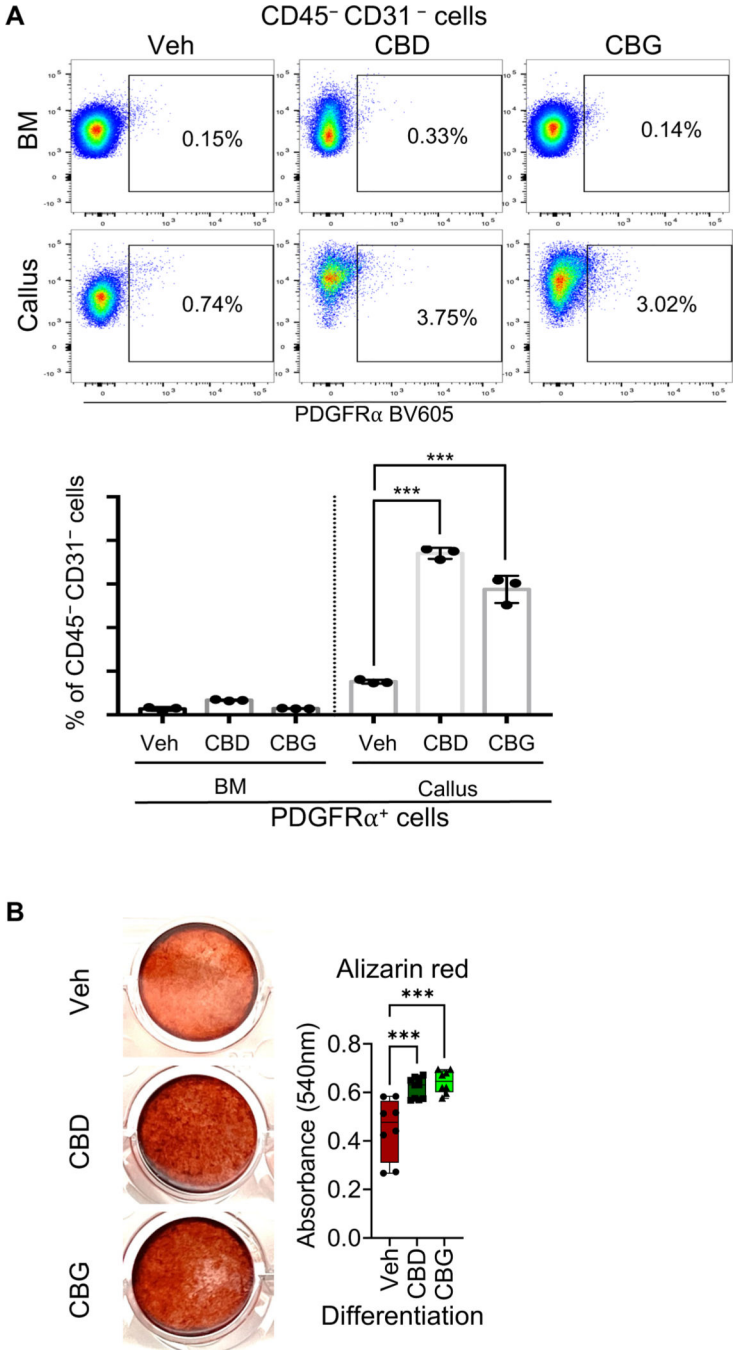

Figure 9. Treatment with CBD or CBG increases the abundance of PDGFRα$^+$ progenitors in the healing callus.

(**A, top**) A representative dot plot of the FC results. The plot shows the abundance of the PDGFRα$^+$ progenitors (i.e., CD45$^-$CD31$^-$ PDGFRα$^+$ cells) in the d3 calli of the mice that were treated with vehicle (Veh), CBD, or CBG. The % of PDGFRα$^+$ progenitors relative to the CD45$^-$CD31$^-$ population in each group is shown. (**A, bottom**) Quantification of the relative proportion (%) of the PDGFRα$^+$ progenitors in the BM and d3 callus. The analysis was performed on mice that were treated with Veh, CBD, or CBG. N = 3, and 4 calli were

pooled in each. (**B, left**) PDGFRα^{+} progenitors were isolated using FACS, and they were subjected to osteogenic differentiation in the presence of Vehicle, 1 μg/ml of CBD, or 1 μg/ml of CBG for 2 weeks. The images show Alizarin Red staining of the differentiated cells. (**B, right**) Quantification of the Alizarin Red staining. N = 8.

The bar graphs present average ± SEM. The box and whiskers plots are presented as min to max and line at median. (***) $P < 0.001$, using one-way ANOVA followed by Tukey's post hoc test.